

Global Optimization of Stacking Sequence in a Laminated Cylindrical Shell Using Differential Quadrature Method

M.R. Saviz^{1,*}, A. Ziaei Asl²

¹Mechanical Engineering Department, Azarbaijan Shahid Madani University, Tabriz, Iran

Received 3 December 2017; accepted 4 February 2018

ABSTRACT

Based on 3-D elasticity approach, differential quadrature method (DQM) in axial direction is adopted along with Globalized Nelder–Mead (GNM) algorithm to optimize the stacking sequence of a laminated cylindrical shell. The anisotropic cylindrical shell has finite length with simply supported boundary conditions. The elasticity approach, combining the state space method and DQM is used to obtain a relatively accurate objective function. Shell thickness is fixed and orientations of layers change in a set of angles. The partial differential equations are reduced to ordinary differential equations with variable coefficients by applying DQM to the equations, then, the equations with variables at discrete points are obtained. Natural frequencies are attained by solving the Eigen-frequency equation, which appears by incorporating boundary conditions into the state equation. A GNM algorithm is devised for optimizing composite lamination. This algorithm is implemented for maximizing the lowest natural frequency of cylindrical shell. The results are presented for stacking sequence optimization of two to five-layered cylindrical shells. Accuracy and convergence of developed formulation is verified by comparing the natural frequencies with the results obtained in the literature. Finally, the effects of mid-radius to thickness ratio, length to mid-radius ratio and number of layers on vibration behavior of optimized shell are investigated. Results are compared with those of Genetic Algorithm (GA) method, showing faster and more accurate convergence.

© 2018 IAU, Arak Branch. All rights reserved.

Keywords: Stacking sequence optimization; Globalized Nelder–Mead; Laminated cylinder; Vibration analysis; Differential quadrature method.

1 INTRODUCTION

LAMINATED composite shells with high-modulus and low density are increasingly demanded in engineering, especially the aerospace industry. However, using this benefit requires the optimization of shape, size and proper placement of fibers within the material, which would be possible by manipulating parameters like, fiber orientation, thickness and number of layers, etc., to extremize objective parameters such as weight, stiffness, strength and dynamic characteristics. The problem is often formulated as a continuous optimization problem with the thickness and orientation of plies as design variables [1], but, for most particular problems, laminate thickness is fixed and fiber orientations are limited to a set of angles so that the design problem becomes a stacking sequence optimization. Haftka and Walsh solved the stacking sequence problem for buckling load maximization [2]. The

*Corresponding author.

E-mail address: saviz@azaruniv.ac.ir (M.R. Saviz).

nonlinear problem, resulting from using ply thicknesses as design variables, is linearized by using ply-orientation identity variables and solved with a branch and bound algorithm. Nagendra solved a similar problem with the addition of strain constraints, through introducing nonlinearities to the problem [3]. Kam and Lai [4] studied the lamination arrangement of moderately thick laminated composite plates for optimal dynamic characteristics via a constrained multi-start global optimization technique. Optimum fiber orientation of shallow shells for maximization of the fundamental frequency is studied by Narita and Zhao [5] through sensitivity analysis with respect to fiber orientation. Moreover, they obtained optimum design of generally laminated rectangular plates having arbitrary boundary conditions with complex method as an extension of the simplex method for more complicated problems [6].

Tsau et al. used simplex method to optimize buckling load of rectangular plates for fiber orientation [7]. The simplex search method was initially developed by Spendley et al. [8], which was subsequently refined by Nelder and Mead [9] for function minimization, then it was followed by Lagarias et al. [10] who addressed convergence behavior of the method. Multi-objective optimization of cylindrical panels based on the first natural frequency and buckling load was studied by Abouhamze and Shakeri [11]. They used Neural Network to model the behavior of structure and Genetic Algorithm for optimization process. Inasmuch as having a number of local optimums is a typical feature of optimization in engineering problems, many researchers have focused on coming up with globalized methods. The main concern, considered in engineering optimization studies is the efficiency of the optimization method. The method should achieve the best design output with best accuracy and minimum cost. This could take place through combining the local and global algorithms. As a result, the hybrid algorithms have recently emerged as an important subject. Margarida and Salcedo [12] combined simulated annealing and simplex method for optimization of continuous nonlinear problems. Also, simplex method is amalgamated with the genetic algorithm [13] as well as the tabu search method [14] by Chelouah and Siarry. Lursen and Riche [15] presented the Globalized Bounded Nelder–Mead method (GNM) in which Nelder–Mead simplex algorithm (as local search method) sequentially becomes global by probabilistic restart. By using this method, they optimized stiffness and buckling load of rectangular plates. A hybrid method combining continuous Tabu search (TS) and Nelder–Mead simplex algorithms for the global optimization of multi-minima functions was presented by Siarry and Chelouah [16]. In addition, exact solutions based on 3-D elasticity equations utilizing trigonometric functions, which are realistic only for the particular case of simply supported cylindrical shells, in spite of their accuracy, reckon with a considerable amount of mathematical complexity. Differential quadrature (DQ) is an efficient mathematical model with relatively low computational cost that has attracted much interest in numerical methods. Bert and Malik [17] presented a review on the early developments in DQM.

Malekzadeh and his co-workers [18, 19] demonstrated that using DQM for solving the governing equations for different mechanical problems leads to highly accurate results with less computation. Generalized DQM was used to study the effects of boundary conditions on the frequency characteristics of a thin rotating cylindrical shell [20]. The analysis was based on Love-type shell theory and the governing equations of motion include the effects of initial hoop tension, centrifugal and Coriolis accelerations due to rotation. Li and Lam [21] used DQ to consider the influence of orthotropic material on the frequency characteristics for a rotating thin truncated circular cross-ply laminated conical shell. Free vibration analysis of laminated conical shells with variable stiffness was presented using the method of DQ [22], using the first-order shear deformation shell theory to account for the effects of transverse shear deformations. A combination of state space method and DQ, based on 2-D elasticity theory, was introduced by Chen et al. [23] to analysis the free vibration of cross-ply laminated beams. They used DQM to determine vibration characteristics of generally laminated beams and cross-ply laminated plates subjected to cylindrical bending.

In this survey, shell thickness is fixed and GNM algorithm is implemented to optimize the fiber orientation of plies in laminated cylindrical shell, based on maximum fundamental natural frequency. The objective frequency function is determined from the free vibration analysis. To solve free vibration equations, the DQM is used based on 3-D elasticity theory. Variable coefficients of governing differential equation are changed to constant ones, using Soong's assumption [24]. The resulted state equations are solved through discretization, by employing DQM in axial direction and solving the Eigen-frequency system of equations. In the optimization problem, the fundamental natural frequency is maximized by determining favorable angle in each layer within the range of $-90 \leq \theta \leq 90$. The procedure requires stacking sequence as input data and provides the value of objective function as output. Accuracy and convergence of developed code is verified by comparing the natural frequencies with the results obtained in the literature. The effects of mid-radius to thickness and length to mid-radius ratios on optimized vibration behavior of shell are investigated. Stacking predictions are compared with the results of Genetic Algorithm (GA) method in terms of convergence speed and accuracy of the optimum, weighting NM with continuous variables against GA with discrete ones.

2 OPTIMIZATION PROBLEM DESCRIPTION

To define the optimization problem, a schematic of stacking sequence problem in a cylindrical shell is shown in Fig. 1.

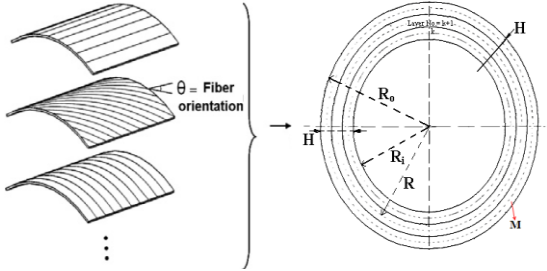


Fig.1
Lamination sequence in a multi-layered cylindrical shell.

The optimization process is responsible for finding the optimal fiber orientation for each layer, within a continuous variable range between -90° and 90° , which is expressed as follows:

$$\omega_{max} = \text{Global Max} \omega(\theta_{opt}) \quad , \quad -90^\circ \leq \theta_{opt} \leq 90^\circ \tag{1}$$

The simplex method which is a free of derivative searcher algorithm, was particularly devised for unconstrained minimization scenarios. Nelder–Mead (simplex) method is a direct search, based on comparison of function values at the $n+1$ vertices of simplex (n is number of design variables), [25]. A simplex of size a (which is typically adapted to the problem characteristics) is initialized at x_0 , establishing the n -dimensional vector space of the coordinates of vertex i , by using the following rule

$$x_i = x_0 + r e_i + \sum_{\substack{k=1 \\ k \neq i}}^n r' e_k \quad i = 1, n, \tag{2a}$$

where e_i is the unit base vector and

$$r = \frac{a}{n\sqrt{2}}(\sqrt{n+1} + n - 1), \quad r' = \frac{a}{n\sqrt{2}}(\sqrt{n+1} - 1) \tag{2b}$$

Fig. 2 shows the schematic outline of the simplex in a 2-D space (an equilateral triangle of side a). The subscripts h, l and s are, in turn, defined as follows:

$$f(x_h) = \max(f(x_i)), f(x_l) = \min(f(x_i)) \text{ and } f(x_s) = \max(f(x_i)), i = 1, \dots, n, \text{ excluding } f(x_h).$$

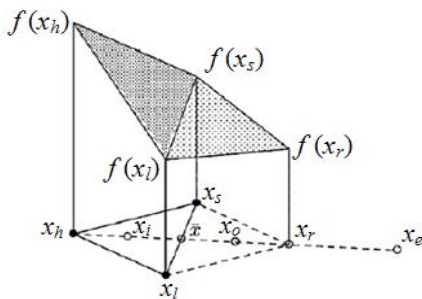


Fig.2
A simplex search algorithm space, [26].

According to the above definition, points x_h, x_l and x_s are depicted in Fig. 2. The objective function $f(x_i)$ is evaluated at each vertex $x_i, i=1, \dots, n + 1$. Afterwards, a new simplex is constructed neighbouring the old one. In minimization case, vertex x_{n+1} , corresponding to the maximum function value is substituted for a better point which

would be nearly located in the negative gradient direction. In order to approach a better point, in the simplex search, trial moves are generated according to four basic operations, namely, reflection, expansion, contraction and multiple contraction (shrinkage), respectively. Using these operations (given in Fig. 3), the simplex improves itself and would eventually arrive at a local optimum point. The algorithm begins with projection of x_h through the mean value of the other x_i 's (\bar{x}) to reach x_r . The point x_r obtained by reflecting away from the worst vertex x_h in the opposite face has the lowest value. If this is the case, a new simplex is constructed by omitting the point x_h from the simplex and including the new point x_r . Again, a new simplex is built from the present one by deleting the vertex corresponding to the highest function value. Since the direction of movement of the simplex is always away from the worst result, the movement would be in a favourable direction. Mathematically, the reflected point x_r is given by

$$x_r = \bar{x} + \alpha(\bar{x} - x_h) \tag{3}$$

\bar{x} is the centroid of all the points x_i , except $i = h$. the reflection coefficient defined as:

$$\alpha = \frac{\text{distance between } x_r \text{ and } \bar{x}}{\text{distance between } x_h \text{ and } \bar{x}}$$

At this stage, four situations might happen, on the basis of the magnitude of $f(x_r)$ with respect to values of $f(x_h)$, $f(x_i)$ and $f(x_s)$.

If in a reflection process $f(x_r) < f(x_i)$ (i.e. if the reflection produces a new minimum), increase the function value further by performing an expansion which creates point x_e , using the relation

$$x_e = \bar{x} + \beta(x_r - \bar{x})$$

β is called the expansion coefficient. Either of x_r or x_e is then maintained as a substitute for x_h , depending on which function value is smaller.

In the case $f(x_i) < f(x_r) < f(x_s)$: x_h is simply replaced with x_r .

If the reflection process gives a point x_r for which $f(x_s) < f(x_r) < f(x_h)$: the simplex is so-called straddled a valley, because by carrying out another simplex operation, simplex would revive to the original one. In this case, x_h is changed for x_r , then contraction operation is conducted towards the best vertex in the new simplex, as follows:

$$x_c = \bar{x} + \gamma(x_h - \bar{x}) \tag{4}$$

$0 \leq \gamma \leq 1$ is called the contraction coefficient. Now, if $f(x_c)$ is less than $f(x_h)$, x_h (late x_r) is substituted for x_c , if not, the simplex would be exposed to a multiple contraction operation, through substituting x_i for $(x_i + x_l) / 2$.

Finally, if $f(x_r) > f(x_h)$: as expected, a shrinkage operation is required. Then, x_h gives its place to x_e , provided that $f(x_e)$ is smaller than $f(x_h)$, otherwise, multiple contraction should be implemented.

$$x_i = (x_i + x_l) / 2 \tag{5}$$

In maximization procedure, everything should be inverted, that is, x_h would be replaced by x_l , and vice versa

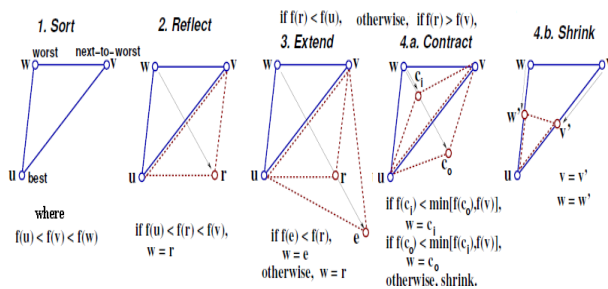


Fig.3 Sequence of steps in one iteration of the Nelder-Mead method, $n = 2$, [26].

The converge of algorithm is controlled using the standard deviation of the function at $n + 1$ vertices of the simplex through the following inequality condition

$$\sqrt{\frac{\sum_{i=1}^{n+1} (f_i - \bar{f})^2}{n}} < \varepsilon \quad (6)$$

$$\text{where } \bar{f} = \frac{1}{n+1} \sum_{i=1}^{n+1} f_i$$

In this study, the tolerance ε , is considered 0.001.

2.1 Present Nelder–Mead simplex method

Luersen and Riche [27] proposed a mixed method for globalized optimization in experiments on analytical test functions and composite laminate design problems. In this method, a multi-dimensional probabilistic function was devised, updating in each trial step to set up a new starting point beyond formerly investigated sections of domain in order to locate the overall optimum more efficiently. A spatial probability of starting a local search is built based on the history of previous local searches. To this end, the following Gaussian Parzen-windows probability function is implemented, [28]

$$p(x) = \frac{1}{N} \sum_{i=1}^N p_i(x) \quad (7a)$$

where, N is the number of points having already been sampled, and $p_i(x)$ is

$$p_i(x) = \frac{1}{(2\pi)^{\frac{n}{2}} \sqrt{(\det[V])}} e^{\left(\frac{1}{2}(x_i - x)^T [V]^{-1} (x - x_i)\right)} \quad (7b)$$

$[V]$ is a diagonal matrix, the elements of which are equal to the square of variances given as follows:

$$V_j = \eta (x_j^{\max} - x_j^{\min})^2 \quad (7c)$$

where η is a positive parameter, which controls the length of the Gaussian. x_j^{\max} and x_j^{\min} are the upper and lower boundaries of the j th direction, respectively. To reduce the numerical cost, N_r points are chosen randomly and the point that maximizes p would be selected to initiate the next search.

In Nelder–Mead search, three start schemes and three convergence criteria are formulated, in addition to the previous convergence criteria given in Eq. (6). In terms of restart schemes, firstly, probabilistic restarts aim at repeating local searches. Small and large restart tests use a small and large simplex of sizes a_s and a_l , as given in Eqs. (2), setting out a new simplex based on the existing best vertex. Depending on the topology of the ending simplex, the following convergence criteria can be applied. Smallness of a simplex is evident, when the following criterion is fulfilled.

$$\max_{k=1, \dots, m} \left(\sum_{i=1}^n \frac{x_i^k}{x_i^{\max} - x_i^{\min}} \right) < \varepsilon_{S1} \quad m = \frac{n(n+1)}{2} \quad (8)$$

where m is the number of simplex edges. Flatness of the simplex is proved based on difference between the highest and lowest values of objective function within vertices of the simplex.

$$|f(x_h) - f(x_l)| < \varepsilon_{S2} \quad (9)$$

Due to poor geometric aspect ratio, a degenerated simplex falls in one sub-space of domain. In other words, a degenerated simplex loses the dimensionality of domain and the vertices lie in the same hyper-plane. Degeneracy of a simplex is checked by either of the following criteria

$$\frac{\min_{k=1,\dots,n} \|e^k\|}{\max_{k=1,\dots,n} \|e^k\|} < \varepsilon_{S3} \quad \text{or} \quad \frac{\det [e]}{\prod_k \|e^k\|} < \varepsilon_{S4} \tag{10}$$

The edge coordinate matrix [e] is a square matrix, comprising of the coordinates of the lines passing through a typical vertex, which is obtained by subtracting coordinates of vertices of an arbitrary edge of the simplex. In a 2-D case, Eqs. (10) are illustrated in Fig. 4.



Fig.4
Two modes of simplex collapse in a 2-D domain.

3 ELASTICITY FORMULATION OF PROBLEM

A laminated hollow cylindrical shell with finite length L , made of m perfectly bonded homogeneous anisotropic composite laminae whose principal axes coincide with three orthogonal coordinate r, θ and z are shown in Fig. 5. The mean radius and the thickness of K_{th} layer are denoted by R_k, h_k ($k = 1, 2, \dots, m$), respectively. The material axis of any layer is not necessarily aligned with the z and θ directions, so the shell conforms to what is generally tailored as a laminated anisotropic shell. The constitutive equations for an arbitrary anisotropic composite layer in reference coordinate system (r, θ, z) are

$$\begin{Bmatrix} \sigma_z \\ \sigma_\theta \\ \sigma_r \\ \tau_{r\theta} \\ \tau_{rz} \\ \tau_{\theta z} \end{Bmatrix} = \begin{bmatrix} C_{11} & C_{12} & C_{13} & 0 & 0 & C_{16} \\ C_{12} & C_{22} & C_{23} & 0 & 0 & C_{26} \\ C_{13} & C_{23} & C_{33} & 0 & 0 & C_{36} \\ 0 & 0 & 0 & C_{44} & C_{45} & 0 \\ 0 & 0 & 0 & C_{45} & C_{55} & 0 \\ C_{16} & C_{26} & C_{36} & 0 & 0 & C_{66} \end{bmatrix} \begin{Bmatrix} \varepsilon_z \\ \varepsilon_\theta \\ \varepsilon_r \\ \gamma_{r\theta} \\ \gamma_{rz} \\ \gamma_{\theta z} \end{Bmatrix} \tag{11}$$

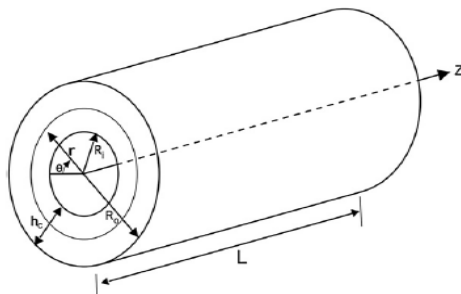


Fig.5
Geometry and coordinates of the laminated shell.

The components of stress (σ) and strain (ε) vectors are given in cylindrical coordinate system and C_{ij} are the material elastic constants. The equations of motion for axisymmetric deformation in the absence of body force are

$$\begin{aligned}
\frac{\partial \sigma_r}{\partial r} + \frac{\sigma_r - \sigma_\theta}{r} + \frac{\partial \tau_{rz}}{\partial z} &= \rho \frac{\partial^2 u_r}{\partial t^2} \\
\frac{\partial \tau_{z\theta}}{\partial z} + \frac{\partial \tau_{r\theta}}{\partial r} + 2 \frac{\tau_{r\theta}}{r} &= \rho \frac{\partial^2 u_\theta}{\partial t^2} \\
\frac{\partial \sigma_z}{\partial z} + \frac{\partial \tau_{rz}}{\partial r} + \frac{1}{r} \tau_{rz} &= \rho \frac{\partial^2 u_z}{\partial t^2}
\end{aligned} \tag{12}$$

where u_r , u_θ and u_z are displacement components and ρ is the mass density of the shell material. The linear axisymmetric strain-displacement relations are written as:

$$\varepsilon_r = u_{r,r} \quad \varepsilon_z = u_{z,z} \quad \gamma_{\theta z} = u_{\theta,z} \quad \varepsilon_\theta = \frac{u_r}{r} \quad \gamma_{r\theta} = \frac{1}{r}(-u_\theta + r u_{\theta,r}) \quad \gamma_{rz} = u_{z,r} + u_{r,z} \tag{13}$$

The stress components σ_z , σ_θ and $\tau_{z\theta}$, include derivatives with respect to axial coordinate. By combining Eqs. (11) and (13), these components are written in terms of displacements. These stresses are expressed in term of the state variables, which are derivative-free relative to z ,

$$\begin{aligned}
\sigma_z &= \frac{C_{13}}{C_{33}} \sigma_r + \left(C_{11} - \frac{C_{13}^2}{C_{33}} \right) \frac{\partial u_z}{\partial z} + \frac{1}{r} \left(C_{12} - \frac{C_{32} C_{13}}{C_{33}} \right) u_r + \left(C_{16} - \frac{C_{36} C_{13}}{C_{33}} \right) \frac{\partial u_\theta}{\partial z} \\
\sigma_\theta &= \frac{C_{23}}{C_{33}} \sigma_r + \left(C_{21} - \frac{C_{23} C_{13}}{C_{33}} \right) \frac{\partial u_z}{\partial z} + \frac{1}{r} \left(C_{22} - \frac{C_{23}^2}{C_{33}} \right) u_r + \left(C_{26} - \frac{C_{36} C_{23}}{C_{33}} \right) \frac{\partial u_\theta}{\partial z} \\
\tau_{\theta z} &= \frac{C_{36}}{C_{33}} \sigma_r + \left(C_{16} - \frac{C_{36} C_{13}}{C_{33}} \right) \frac{\partial u_z}{\partial z} + \left(C_{66} - \frac{C_{36}^2}{C_{33}} \right) \frac{\partial u_\theta}{\partial z} + \frac{1}{r} \left(C_{26} - \frac{C_{36} C_{23}}{C_{33}} \right) u_r
\end{aligned} \tag{14}$$

The following approximation, introducing radial local coordinate ξ_k , located at the centre of K_{th} sub-layer is made in governing Eqs. (12) to (14),

$$\xi_k = r - R_k \quad , \quad \eta_k = \frac{\xi_k}{R_k} \Rightarrow \eta_k = \frac{r}{R_k} - 1 \Rightarrow \frac{1}{r} = \frac{1}{R_k} \cdot (1 - \eta_k) \Rightarrow \frac{1}{r^2} = \frac{1}{R_k^2} \cdot (1 - 2\eta_k) \tag{15a}$$

where η is non-dimensional radial coordinate, R_k is the mid-radius of K_{th} sub-layer. Assuming each sub-layer as a thin coaxial shell results in

$$\eta_k = \frac{\xi_k}{R_k} \ll 1 \Rightarrow \frac{1}{r} = \frac{1}{R_k} \quad , \quad \frac{1}{r^2} = \frac{1}{R_k^2} \quad , \quad \frac{\partial}{\partial r} = \frac{1}{R_k} \cdot \frac{\partial}{\partial \eta} \quad , \quad \frac{\partial^2}{\partial r^2} = \frac{1}{R_k^2} \cdot \frac{\partial^2}{\partial \eta^2} \tag{15b}$$

Furthermore, in order to study the free vibration, the displacements and hence the stresses are considered as harmonic functions,

$$\begin{aligned}
\sigma_r &= \bar{\sigma}_r(\eta, z) e^{i\omega t} & u_r &= \bar{u}_r(\eta, z) e^{i\omega t} \\
\sigma_z &= \bar{\sigma}_z(\eta, z) e^{i\omega t} & u_\theta &= \bar{u}_\theta(\eta, z) e^{i\omega t} \\
\sigma_\theta &= \bar{\sigma}_\theta(\eta, z) e^{i\omega t} & u_z &= \bar{u}_z(\eta, z) e^{i\omega t} \\
\tau_{r\theta} &= \bar{\tau}_{r\theta}(\eta, z) e^{i\omega t} & \tau_{rz} &= \bar{\tau}_{rz}(\eta, z) e^{i\omega t} \\
\tau_{\theta z} &= \bar{\tau}_{\theta z}(\eta, z) e^{i\omega t} & &
\end{aligned} \tag{16}$$

By applying Eqs. (14), (15) and (16) into Eqs. (12), keeping the terms having radial derivatives, as the state vector on the right side and taking the terms having axial derivatives to the left side, the governing equations of motion are written in the following form

$$\frac{d\{S\}}{d\eta} = [A]\{S\} \quad (17)$$

$\{S\} = \{\bar{\sigma}_r, \bar{u}_z, \bar{u}_\theta, \bar{u}_r, \bar{\tau}_{rz}, \bar{\tau}_{r\theta}\}^T$ is the vector of state variables. The approximations of Eqs. (15) are literally implemented to convert variable coefficients in components of $[A]$ into the constant ones. The matrix of coefficients is,

$$[A] = \begin{bmatrix} a_1 & a_2 \frac{\partial}{\partial x} & a_3 \frac{\partial}{\partial x} & a_4 - \rho R \omega^2 & -R \frac{\partial}{\partial x} & 0 \\ 0 & 0 & 0 & -R \frac{\partial}{\partial x} & -a_6 & a_7 \\ 0 & 0 & 1 & 0 & a_7 & -a_8 \\ a_9 & -a_{10} \frac{\partial}{\partial x} & -a_{11} \frac{\partial}{\partial x} & -a_{12} & 0 & 0 \\ -a_{10} \frac{\partial}{\partial x} & a_{13} \frac{\partial^2}{\partial x^2} - \rho R \omega^2 & a_{14} \frac{\partial^2}{\partial x^2} & -a_2 \frac{\partial}{\partial x} & -1 & 0 \\ -a_{11} \frac{\partial}{\partial x} & a_{14} \frac{\partial^2}{\partial x^2} & a_{16} \frac{\partial^2}{\partial x^2} - \rho R \omega^2 & -a_3 \frac{\partial}{\partial x} & 0 & -2 \end{bmatrix} \quad (18)$$

where, a_i ($i=1\dots 10$) are constant coefficients, determined by using the boundary condition.

3.1 Semi-analytical DQM solution

In order to obtain the solution for the state space form of governing equations (Eq. (17)) of the laminated shell, a semi-analytical procedure applying DQ technique is developed. In this study, the boundary conditions for simply supported (S-S) cylindrical shell at the end edges ($z=0, L$) are considered as follows:

$$\text{S-S: } \bar{u}_r = \bar{u}_\theta = \bar{\sigma}_z = 0 \quad \text{at } z = 0, L \quad (19)$$

In DQM, the n th-order partial derivative of a continuous function $f(x, z)$ is approximated relative to x at a given point x_i , as a linear summation of weighted function values at all of the discrete points in the domain of variable x

$$\left. \frac{\partial f^n(x, z)}{\partial x^n} \right|_{x=x_i} = \sum_{j=1}^N g_{ij}^n f(x_j, z) \quad (i = 1, 2, \dots, N; n = 1, 2, \dots, N-1) \quad (20)$$

where N is the number of sampling points, and g_{ij}^n are the x_i -dependent weighting coefficients [28]. By inserting Eq. (20) into Eq. (17), the following state space equations are derived for each composite sub-layer, in terms of the state variables at every single sampling point for any given lamina

$$\begin{aligned} \frac{\partial \bar{\sigma}_r}{\partial \eta} &= \left(\frac{C_{23}}{C_{33}} - 1 \right) \bar{\sigma}_r + \left(\frac{C_{22}}{R} - \rho R \omega^2 - \frac{C_{23}^2}{RC_{33}} \right) \bar{u}_r + \left(C_{12} - \frac{C_{23}C_{13}}{C_{33}} \right) \sum_{j=1}^N g_{ij} \bar{u}_{zj} + \left(C_{26} - \frac{C_{23}C_{36}}{C_{33}} \right) \sum_{j=1}^N g_{ij} \bar{u}_{\theta j} - R \sum_{j=1}^N g_{ij} \bar{\tau}_{rzj} \\ \frac{\partial \bar{u}_{zi}}{\partial \eta} &= \left(\frac{RC_{44}}{C_{45}^2 - C_{44}C_{55}} + \frac{RC_{45}}{C_{45}^2 - C_{44}C_{55}} \right) \bar{\tau}_{rzi} - R \sum_{j=1}^N g_{ij} \bar{u}_{zj} \\ \frac{\partial \bar{u}_{\theta i}}{\partial \eta} &= \bar{u}_{\theta i} + \frac{RC_{45}}{C_{45}^2 - C_{44}C_{55}} \bar{\tau}_{rzi} - \frac{RC_{55}}{C_{45}^2 - C_{44}C_{55}} \bar{\tau}_{r\theta i} \end{aligned} \quad (21)$$

where, subscript $()_i$ denotes the function value at the grid point i . Similarly, the secondary variables, Eqs. (14), are discretized as follows:

$$\begin{aligned}\bar{\sigma}_{zi} &= \frac{C_{13}}{C_{33}} \bar{\sigma}_{ri} + \left(C_{11} - \frac{C_{13}^2}{C_{33}} \right) \sum_{j=1}^N g_{ij} \bar{u}_{zj} + \left(C_{16} - \frac{C_{13}C_{36}}{C_{33}} \right) \sum_{j=1}^N g_{ij} \bar{u}_{\theta j} + \frac{1}{R} \left(C_{12} - \frac{C_{13}C_{23}}{C_{33}} \right) \bar{u}_{ri} \\ \bar{\sigma}_{\theta i} &= \frac{C_{23}}{C_{33}} \bar{\sigma}_{ri} + \left(C_{12} - \frac{C_{13}C_{23}}{C_{33}} \right) \sum_{j=1}^N g_{ij} \bar{u}_{zj} + \left(C_{26} - \frac{C_{23}C_{36}}{C_{33}} \right) \sum_{j=1}^N g_{ij} \bar{u}_{\theta j} + \frac{1}{R} \left(C_{22} - \frac{C_{23}^2}{C_{33}} \right) \bar{u}_{ri}\end{aligned}\quad (22)$$

By assembling Eqs. (21) for all grid points, the following discretized form of state equations would be obtained

$$\frac{d}{d\eta} \{A\} = [M] \{A\} \quad (23)$$

where

$$\{A_k\} = [\{\bar{\sigma}_{ri}\} \ \{\bar{u}_{zi}\} \ \{\bar{u}_{\theta i}\} \ \{\bar{u}_{ri}\} \ \{\bar{\tau}_{rzi}\} \ \{\bar{\tau}_{r\theta i}\}]^T, \quad \{\bar{\sigma}_{ri}\} = [\bar{\sigma}_{r_1} \ \bar{\sigma}_{r_2} \ \dots \ \bar{\sigma}_{r_N}]^T \quad (24)$$

By expressing the boundary conditions at $z=0, L$ (Eq. (19)) in terms of discrete variables on boundary nodes and incorporating them into Eq. (23), a system of algebraic global state equations would appear as follows:

$$\frac{d}{d\eta} \{A_b\} = [M_b] \{A_b\} \quad (25)$$

where, $\{A_b\}$ contains the unknown variables on the boundaries. Now, the unknown state variables in $\{A_k\}$ are obtained. The standard solution of Eq. (25), delivers the following unique answer for the state variables, in terms of the calculated values in the previous sub-layer,

$$\{A_b(\eta_k)\} = e^{(M_b)(\eta_k - \eta_{k-1})} \{A_b(\eta_{k-1})\}, \quad -\frac{h_k}{2R_K} \leq \eta \leq \frac{h_k}{2R_K} \quad (26)$$

The above response can be written in terms of K^{th} , and $(K+1)^{\text{th}}$ sub-layer properties

$$\{A_b(\eta_{k+1})\} = e^{(M_b^{k+1})h_{k+1}} e^{(M_b^k)h_k} \{A_b(\eta_{k-1})\} \quad k = 1, 2, \dots, m-1 \quad (27)$$

By extending the above relation to all the m layers in the thickness, the relation between the entities at the inner and outer surfaces are obtained

$$\{A_b|_{r=R_o}\} = [T_b] \{A_b|_{r=R_i}\} \quad (28a)$$

where, the global transfer matrix is

$$[T_b] = \prod_{k=m}^1 e^{(M_b^k)h_k} \quad (28b)$$

Finally, for free vibration analysis, the outer and inner surfaces of shell should be traction free as follows:

$$\bar{\tau}_{rz} = \bar{\tau}_{r\theta} = \bar{\sigma}_r = 0 \quad \text{at } r = R_i \text{ and } R_o \quad (29)$$

By incorporating Eq. (29) into the global unknown state vector, in Eqs. (28), the following Eigen-frequency system of equations emerges

$$\text{Det} [T_{ij}] = 0 \quad i = 1, 5, 6 ; j = 2, 3, 4 \quad (30)$$

where, T_{ij} are partitioned matrices of T_b . Solving the system of Eqs. (30) yields the natural frequencies. Therefore, the lowest natural frequency of the laminate can be expressed in terms of the fiber orientations within each layer, (θ_i) as follows:

$$\omega = F(\theta_1, \theta_2, \theta_3, \dots, \theta_m)$$

This is the fitness function that should be optimized for obtaining the maximum first natural frequency.

4 NUMERICAL RESULTS AND DISCUSSION

For numerical analysis purpose, sampling points in axial direction (Eq. (24)) are extracted with the following coordinates, [29]

$$z_i = \left(1 - \cos \frac{(i-1)\pi}{N-1}\right) \frac{L}{2}, \quad i = 1, 2, \dots, N \quad (31)$$

4.1 Free vibration analysis

To validate the accuracy of the present approach for free vibration analysis, a three-layered shell with $[90^\circ / 0^\circ / 90^\circ]$ lay-up and simply supported boundary conditions with the following lamina mechanical parameters is considered

$$E_\theta = E_r = 7.6 \text{ GPa}, E_{zz} = 19.1 \text{ GPa}, G_{rz} = G_{\theta z} = 4.1 \text{ GPa}, \nu_{rz} = \nu_{\theta z} = 0.26, \rho = 1643 \text{ kg/m}^3$$

The thickness ratio is $S = R/h = 500$, and the following non-dimensional natural frequency is defined in order to compare the results with those obtained by Lam and Loy [30] and Zhang [31], given in Table 2., for the following natural frequency parameter.

$$\omega^* = \omega R \sqrt{\frac{\rho}{E_\theta}} \quad (32)$$

According to Table 1., there is a good agreement, that is, the difference between the present results and those of the Refs. [30] and [31] tends to decline by increasing the aspect ratio L/R .

Table 1
Comparison between non-dim. Natural frequencies.

L/R	Present	Ref [20]	Ref [21]
1	1.061287	1.061284	1.061281
5	0.248638	0.248635	0.248634
10	0.083909	0.083908	0.083907
20	0.023593	0.023590	0.023589

Secondly, the solution for the axisymmetric free vibration of an isotropic cylinder is evaluated; to demonstrate the efficiency and versatility of the present formulations, the results are compared with those reported by Khalili et al. [32]. A wide range of R/h and h/L ratios are investigated.

To study the convergence rate of the present method, numerical results are presented for laminated cylindrical shells with $[45^\circ]$, $[-45^\circ / 45^\circ]$ and $[-45^\circ / 45^\circ / -45^\circ]$ stacking sequences. The shells have different boundary conditions with the length ratio $L/R = 1$, thickness ratio is $S = 10$, and plies are made of unidirectional fibrous composite material with equal thickness and the following material properties

$$E_{\theta} = E_r = 6.9 \text{ GPa}, E_{zz} = 40 E_{\theta}, G_{rz} = G_{\theta z} = 0.5 E_{\theta}, \nu_{rz} = 0.49, \nu_{\theta z} = 0.25, \rho = 1580 \text{ kg / m}^3$$

First three natural frequencies for above three cylindrical shells are presented in Table 2. As expected, natural frequencies vary from the maximum value to the minimum value. This table also demonstrates that increasing the number of layers leads to an increase in the stiffness of the shells and consequently rises in the natural frequencies.

Table 2
Convergence of natural frequencies for three laminations & modes (Hz).

	Mode No. (n)	1	2	3
[45°]	N = 5	1514.37	8168.45	8862.63
	N = 8	1611.27	8275.34	9035.86
	N=10	1618.91	8281.52	9046.05
[-45°/45°]	N = 5	1652.03	8713.61	9797.55
	N = 8	1709.35	8907.28	10017.91
	N=10	1719.54	8930.14	10243.36
[-45°/45°/-45°]	N = 5	1701.71	8731.44	10663.69
	N = 8	1848.19	9033.31	11541.25
	N=10	1859.65	9146.68	11658.48

The effect of the geometry such as thickness and length on the fundamental frequencies of the above single layer shell with S-S boundary condition are given in Table 3.

Table 3
The effect of shell geometry on fundamental frequencies.

S = 4	L/R= 0.3	3070.06
	L/R= 1.0	2252.05
	L/R= 2.5	1797.01
S =10	L/R= 0.3	2799.81
	L/R= 1.0	1618.91
	L/R= 2.5	1268.93
S =30	L/R= 0.3	2285.52
	L/R= 1.0	1470.71
	L/R= 2.5	1023.02

As expected, for shorter shells the natural frequencies are considerably bigger than those of the long ones. The biggest natural frequency belongs to the thick and shortest shell and vice versa. For longer shells, the thickness ratio has a smaller effect on natural frequency. Because of the same density and elastic modulus of layers, the variations of natural frequencies with thickness and length of shell has similar trend.

4.2 Optimization results

To verify the capability of the local searcher in finding the optimum point, a two dimensional analytical function, so-called Rosenbrock with a famous minimum at $x=(1, 1)$ is taken to be optimized. Fig. 6 shows the way simplex vertices progressively approach the minima through performing simplex operations. The process starts with the initial simplex in which vertexes are 2 and 3, constructed on point 1 (-2, -1). Also, the downward trend in the fitness function calculated in the vertexes having the minimum values (started at point 2), versus number of steps is given in Fig. 7.

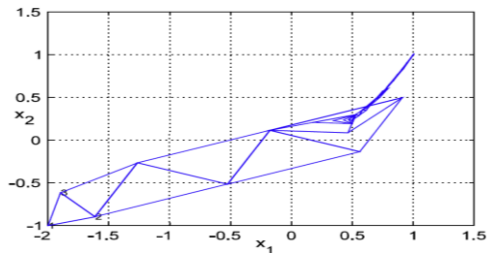


Fig.6
Simplexes in search for the minimum of Rosenbrock function.

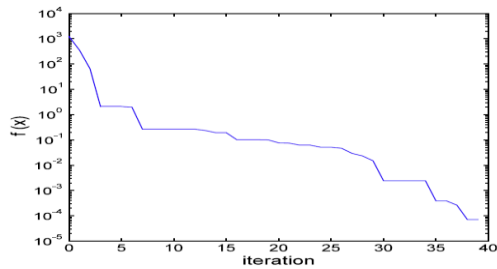


Fig.7
Improving trend in objective function value.

As it is seen the function has reached its minimum value after 39 evaluations. The values of used parameters in the optimization algorithm are provided in Table 4.

Table 4
Parameters of optimization algorithm.

ε_{S1}	0.009
ε_{S2}	1.0e-05
$\varepsilon_{S3}, \varepsilon_{S4}$	0.04
α	0.01
N_r	10
E_{max}	1000
a	10°
a_l	15°
a_s	5°

Firstly, the ply arrangement in a simply-supported (S-S) three-layered cylindrical shell with the following properties is optimized:

$$E_{zz} = 84.9 \text{ GPa}, E_{\theta} = E_r = E_{zz} / 40, G_{zr} / E_{zz} = 0.6, G_{r\theta} / E_{zz} = 0.5, \nu_{zr} = 0.25, \nu_{r\theta} = 0.32, \rho = 1408 \text{ kg} / \text{m}^3$$

In order to have further verification for the whole formulation and solution method, a comparison has been made with similar results obtained by Shakeri et al. [33], in which a Genetic Algorithm approach has been used. For three-layered shell with $L/R = 1$ and thickness ratio $S = 10$, the incremental trend in fundamental frequency with the number of GA generation is given in Fig 8.

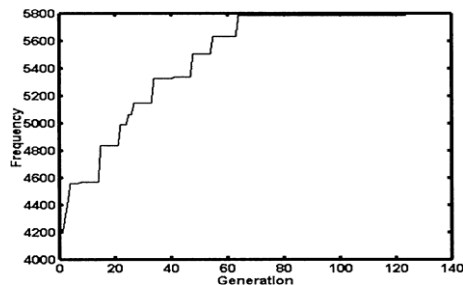


Fig.8
Convergence of natural frequency for GA, three-layer shell, [33].

It is observed from this convergency chart that the natural frequency reaches 5774.1 Hz, not earlier than 61 generations, which have been evaluated through 150 runs.

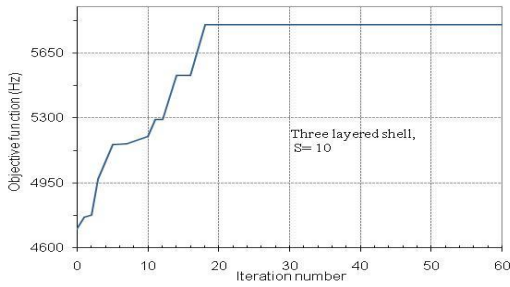


Fig.9
Objective function changes for S-S shell with three layers, S=10.

By comparing this graph with Fig. 9, it is inferred that the convergence rate of GNM method towards the solution is over three times faster than that of GA, so that, its computation effort would be less than GA. It is also concluded that GNM overestimates the three variable fitness function, as much as 25.3 Hz. This finding is consistent with the fact that the present approach avoids entrapment in local maxima and finds near-optimal results. On the other hand, if the GA reaches a population well-distributed within the solution space at the beginning of the search, it would localize the promising zones more quickly, however, its improvement rate towards the optimal stacking, as a local searcher is slower. In other words, this optimization method deals with ply angles one at a time and does not consider interaction of ply angles. Secondly, the simply-supported (S-S) cylinders with two, three and four layers are considered, the layers of which are constructed of unidirectional fibre reinforced graphite-epoxy with the following properties:

$$E_{\theta} = E_r = 6.57 \text{ GPa}, E_{zz} = 156.0 \text{ GPa}, G_{rz} = 5.47 \text{ GPa}, G_{r\theta} = 3.92 \text{ GPa}, \nu_{rz} = 0.27, \nu_{r\theta} = 0.49, \rho = 1408 \text{ kg/ m}^3$$

A two-layered laminated cylindrical shell with $L/R = 2$ and thickness ratios $S = 10, 20, 100$ is taken into account. In this case, there are two continuous design variables, namely, the ply orientations, which are bounded between -90° and 90° . For two layered cylinder with $S=10$, Fig. 10 shows the simplexes developed during the best diversification process within ten initializations, moving towards the optimal stacking sequence $[71.712^\circ, 72.415^\circ]$. The process has taken 15 evaluations, however, it occupies 10 promising triangles. The evaluation process stops after a number of successive iterations without detecting any new promising vertex in the area.

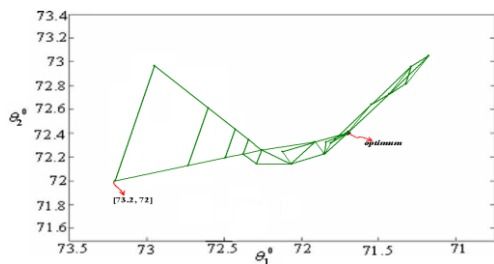


Fig.10
Path followed during the intensification in Nelder–Mead method.

As it is illustrated in Fig. 11, the maximum base natural frequency is achieved in the ninth evaluation, which equals 7189.6 Hz.

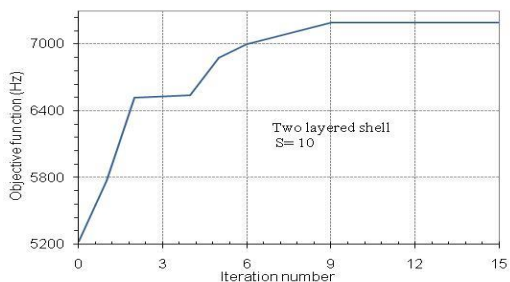


Fig.11
Objective function changes for S-S shell with two layers, S=10.

By taking three-layered shell into consideration, three continuous design variables would be recognized. The changes in objective function with number of iterations for thick shell with $S=10$ is shown in Fig. 12, indicating the convergence of the objective function.

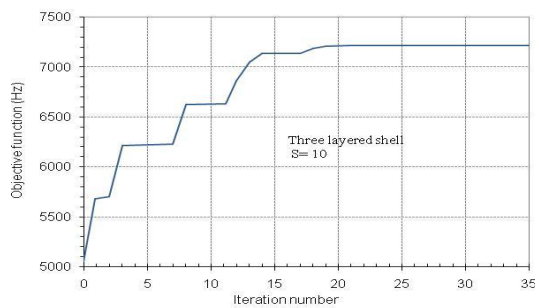


Fig.12
Objective function changes for S-S shell with three layers, $S=10$.

It is observed that the maximum value of the lowest frequency is obtained after 21 evaluations. The optimum stacking sequence is $[69.17^\circ, 64.63^\circ, -38.51^\circ]$ and the corresponding maximum natural frequency is obtained as 7213.8 Hz . In this figure, GNM has been interrupted after 35 evaluations without any improvement in fundamental frequency. Once the optimal stacking sequence is achieved, based on the local maximum values, a list of ten angle sets along with the corresponding natural frequencies has been provided in Table 5., namely, the promising list.

Table 5
Promising list for ten runs, three-layer, S-S, $S=10$.

Number of run N_r	Local optimum stacking sequence, degree°			Local max. objective function (Hz)
1	72.74	67.35	-69.98	7085.6
2	-1.39	-63.75	59.05	6367.2
3	61.68	-41.33	-74.68	6907.5
4	73.37	-84.29	-74.54	6821.9
5	-0.05	-63.68	-1.16	6576.1
6	-0.15	-63.91	29.44	6576.2
7	1.37	-65.45	63.67	6422.3
8	69.17	64.63	-38.51	7213.8
9	-0.10	-56.17	41.73	6581.9
10	0.26	-65.52	-61.77	6352.1

In this table, the eighth set of local results is highlighted due to having the maximum natural frequency. By using the promising list, the optimal solution is identified far from the starting point, in association with the global search for optimized stacking sequence. Figs. 13 and 14 give pictures of the ascending trend in fitness functions versus the number of iterations during the most promising evaluation process for relatively thinner three-layered cylinders with $S=20$ and 100, respectively.

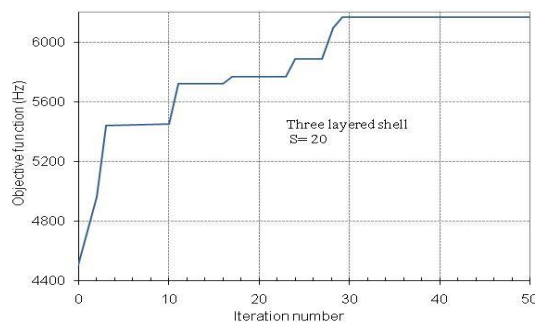
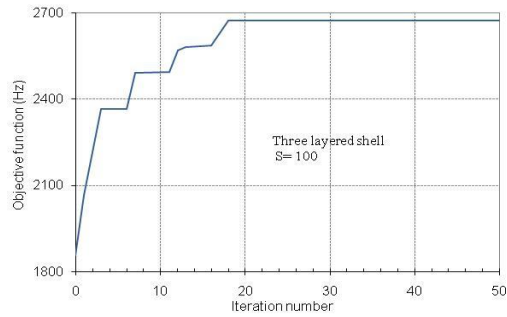
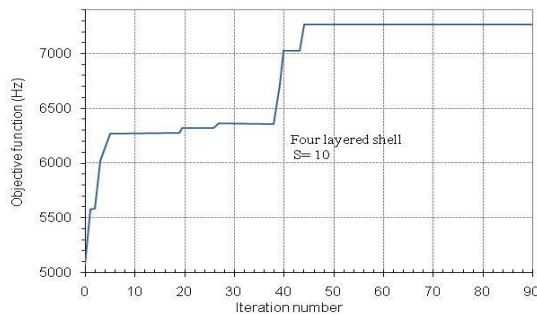


Fig.13
Objective function changes for S-S shell with three layers, $S=20$.

**Fig.14**

Objective function changes for S-S shell with three layers, $S=100$.

The optimal solutions are obtained when the values of fundamental frequency reach 6172.3 and 2674.5 Hz after 29 and 18 evaluations, respectively. The corresponding optimal stacking sequences for $S = 20$ and 100 are $[-70.82^\circ, -56.39^\circ, 36.18^\circ]$ and $[-70.23^\circ, -62.51^\circ, 36.62^\circ]$, respectively. At this stage, the lamination sequence in four-layered composite cylindrical shell with the aforementioned material and geometrical properties is optimized. The thickness-wise arrangement of layers should be found in terms of ply orientations, which are bounded between -90° and 90° . The results are presented for three different S ratios. In Fig. 15 the history of fitness function with respect to iteration number is shown for $S = 10$.

**Fig.15**

Objective function changes for S-S shell with four layers, $S=10$.

The highest natural frequency for this structure is 7265.4 Hz , which is attained after performing 44 operations and with this regard the optimal stacking sequence is $[-43.71^\circ, 47.85^\circ, -68.04^\circ, 39.53^\circ]$.

According to this figure, GNM has been interrupted after 90 evaluations without improvement in the result. The optimization results for ten local searches of the highest natural frequency are contents of the promising list, given in Table 6., along with the corresponding optimal stacking sequences.

Table 6

Promising list for ten runs, four-layer, S-S, $S = 10$.

Number of run N_r	Local optimum for stacking sequence , degree°				Local max. objective function (Hz)
1	85.18	-64.83	64.87	1.71	6307.4
2	-71.04	75.42	-84.37	63.45	6355.2
3	-64.18	64.39	-62.86	62.64	6270.6
4	-63.85	62.98	-59.03	60.73	6272.9
5	78.66	-65.07	61.85	-2.34	6310.3
6	-43.71	47.85	-68.04	39.53	7265.4
7	-72.82	72.96	-72.68	71.93	7017.1
8	-62.62	62.20	-60.25	56.32	6265.7
9	-65.57	61.25	-65.54	56.96	7017.2
10	62.69	-65.56	57.04	-3.34	6260.8

The convergence histories of lowest natural frequency for four-layered cylinders with $S = 20$ and 100 are illustrated in Figs. 16 and 17, respectively.

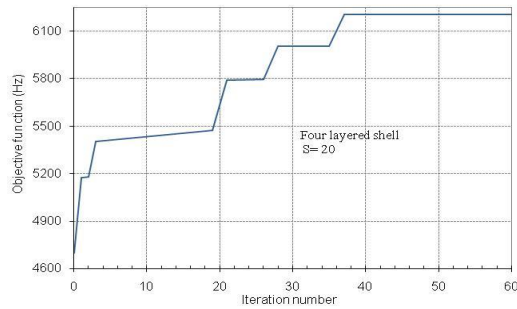


Fig.16
Objective function changes for S-S shell with four layers, $S=20$.

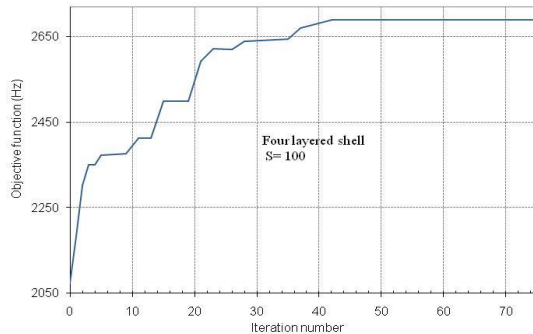


Fig.17
Objective function changes for S-S shell with four layers, $S=100$.

According to these graphs, the optimum solutions for relatively thick and thin shells are achieved when the frequency function become 6204.7 and 2895.1 Hz, respectively. These values can be obtained after 37 and 42 evaluations, and the corresponding optimal laminations are obtained as $[71.05^\circ, 57.11^\circ, -43.22^\circ, 69.42^\circ]$ for $S = 20$, and $[70.47^\circ, 66.23^\circ, -49.54^\circ, -73.02^\circ]$ for $S = 100$.

In GNM method, termination criteria are constrained by the maximum number of evaluations of frequency function (E_{max}). In order to study the effect of E_{max} on the accuracy of optimum solution for four layered simply supported cylindrical shell with $S = 10$, the globally optimized goal functions, determined in each single run are weighted against each other. For this purpose, values of the maximum frequency function in 10 independent runs are presented in Fig. 18. It is worth noting that, by setting $E_{max} = 1000$, the results of all runs are relatively near the optimum one, while for the other values of E_{max} , smaller than 1000, the optimum frequencies are rather scattered, and there is less opportunity to achieve the optimal answer in just a few runs.

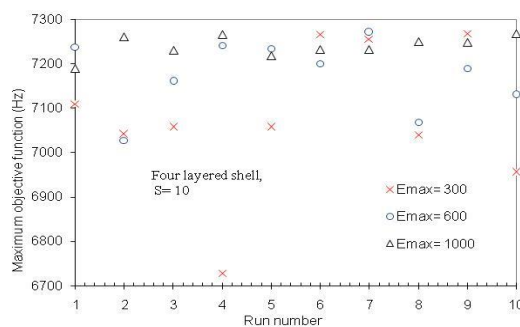


Fig.18
Maximum objective functions for 10 independent runs.

5 CONCLUSIONS

The optimization of stacking sequence for a laminated cylindrical shell, based on maximum lowest frequency is carried out, by making use of GNM algorithm. This study demonstrates that the 3-D elasticity state equations mixed with DQM is capable of an accurate vibration analysis on laminated shell. The effectiveness of the method in

calculating the vibrational behaviour of shell was tested by comparing the numerical results with the related published ones in literature. The following observations are made from the above studies:

- In equal cylinder diameters, both the length ratio and thickness ratio have positive influence on natural frequency. However, the former one seems to be more effective.
- By using the promising list, it is observed that the optimal solution is quite possible to be far from the starting point. The performance level of Nelder–Mead algorithm with respect to convergence speed and accuracy is enhanced, in association with the globalized search for optimized stacking sequence, by virtue of avoiding entrapment in local maximum results.
- In every case study, the reliable amount for the maximum number of objective function evaluations, made before termination of GNM search (E_{\max}) should be determined. By setting E_{\max} to this number, there would be more opportunity to achieve the optimal answer in just a few runs.
- The lowest natural frequency of optimized shell depends on the number of shell layers. Besides, the frequency parameter decreases more rapidly for the shell having more number of layers, and tends to remain constant for thin shell.
- Results of GNM method are compared with corresponding outcomes of the GA method, delivering satisfactory convergence, as well as good agreement both in terms of numerical cost and accuracy, in addition to the drawback that the variables in GA are discrete. It can be concluded that in spite of GA, GNM is not dependent on the initiation point.
- DQM is implemented to overcome the intricacy addressed by the 3-D elasticity methods, when it comes to optimization of lamination sequence in laminated cylindrical shell.

REFERENCES

- [1] Schmit L.A., 1979, Optimum design of laminated fiber composite plates, *International Journal for Numerical Methods in Engineering* **11**: 623-640.
- [2] Haftka R.T., Walsh J.L., 1992, Stacking sequence optimization for buckling of laminated plates by integer programming, *AIAA Journal* **30**: 814-819.
- [3] Nagendra S., Haftka R.T., Gurdal Z., 1992, Stacking sequence of simply supported laminated with stability and strain constraints, *AIAA Journal* **30**: 2132-2137.
- [4] Kam T.Y., Lai F.M., 1995, Design of laminated composite plates for optimal dynamic characteristics using a constrained global optimization technique, *Computer Methods in Applied Mechanics and Engineering* **20**(3-4): 384-402.
- [5] Narita Y., Zhao X., 1998, An optimal design for the maximum fundamental frequency of laminated shallow shells, *International Journal of Solids and Structures* **35**(20): 2571-2583.
- [6] Narita Y., Zhao X., 1997, Maximization of fundamental frequency for generally laminated rectangular plates by the complex method, *Transaction of the Japan Society of Mechanical Engineers Part C* **63**: 364-370.
- [7] Tsau L.R., Chang Y.H., Tsao F.L., 1995, The design of optimal stacking sequence for laminated FRP plates with inplane loading, *Computers & Structures* **55**(4): 565-580.
- [8] Spendley W., Hext G.R., Himsforth F.R., 1962, Sequential application of simplex designs in optimization and evolutionary operation, *Techno Metrics* **4**: 441-461.
- [9] Nelder J.A., Mead R., 1965, A simplex for function minimization, *The Computer Journal* **7**: 308-313.
- [10] Lagarias J.C., Reeds J.A., Wright M.H., Wright P.E., 1999, Convergence behavior of the Nelder–Mead simplex algorithm in low dimensions, *The SIAM Journal on Optimization* **9**: 112-147.
- [11] Abouhamze M., Shakeri M., 2007, Multi-objective stacking sequence optimization of laminated cylindrical panels using a genetic algorithm and neural networks, *Composite Structures* **81**: 253-263.
- [12] Margarida F.C., Salcedo R.L., 1996, The simplex-simulated annealing approach to continuous non-linear optimization, *Computers & Chemical Engineering* **20**(9): 1065-1080.
- [13] Chelouah R., Siarry P., 2003, Genetic and Nelder–Mead algorithms hybridized for a more accurate global optimization of continuous multimimima functions, *The European Journal of Operational Research* **148**: 335-348.
- [14] Chelouah R., Siarry P., 2005, A hybrid method combining continuous tabu search and Nelder–Mead simplex algorithms for the global optimization of multimimima functions, *The European Journal of Operational Research* **161**: 636-654.
- [15] Luersen M.A., Riche R.L., 2004, Globalized Nelder–Mead method for engineering optimization, *Computers & Structures* **82**: 2251-2260.
- [16] Siarry P., Chelouah R., 2005, A hybrid method combining continuous Tabu search and Nelder–Mead simplex algorithms for the global optimization of multimimima functions, *The European Journal of Operational Research* **161**: 634-654.

- [17] Bert C.W., Malik M., 1997, Differential quadrature method: a powerful new technique for analysis of composite structures, *Composite Structures* **39**: 179-189.
- [18] Malekzadeh P., Farid M., Zahedinejad P., 2008, A three-dimensional layer wise differential quadrature free vibration analysis of laminated cylindrical shells, *International Journal of Pressure Vessels and Piping* **85**: 450-458.
- [19] Malekzadeh P., Fiouz A.R., Razi H., 2009, Three-dimensional dynamic analysis of laminated composite plates subjected to moving load, *Composite Structures* **90**: 105-114.
- [20] Li H., Lam K.Y., 1998, Frequency characteristics of a thin rotating cylindrical shell using the generalized differential quadrature method, *International Journal of Mechanical Sciences* **40**(5): 443-459.
- [21] Li H., Lam K.Y., 2001, Orthotropic influence on frequency characteristics of a rotating composite laminated conical shell by the generalized differential quadrature method, *International Journal of Solids and Structures* **38**: 3995-4015.
- [22] Wu C.P., Lee C.Y., 2001, Differential quadrature solution for the free vibration analysis of laminated conical shells with variable stiffness, *International Journal of Mechanical Sciences* **43**(8): 1853-1869.
- [23] Chen W.Q., Lv C.F., Bian Z.G., 2003, Elasticity solution for free vibration of laminated beams, *Composite Structures* **62**: 75-82.
- [24] Soong T.V., 1970, A subdivisional method for linear system, *AIAA/ASME Structures* **1970**: 211-223.
- [25] Duda O.R., Hart P.E., Strol D.G., 2001, *Pattern Classification*, New York, John Wiley & Sons.
- [26] Gilli M., Winker P., 2003, A global optimization heuristic for estimating agent based models, *Computational Statistics and Data Analysis* **42**: 299-312.
- [27] Luersen M.A., Riche R.L., 2004, Globalized Nelder–Mead method for engineering optimization, *Computers & Structures* **82**: 2251-2260.
- [28] Shu C., Richards B.E., 1992, Application of generalized differential quadrature to solve two-dimensional incompressible Navier–Stokes equations, *International Journal for Numerical Methods in Fluids* **15**: 791-798.
- [29] Chen W.Q., Lu C.F., 2005, 3D free vibration analysis of cross-ply laminated plates with one pair of opposite edges simply supported, *Composite Structures* **69**: 77-87.
- [30] Lam K.Y., Loy C.T., 1995, Analysis of rotating laminated cylindrical shells by different thin shell theories, *Journal of Sound and Vibration* **1995**: 23-35.
- [31] Zhang X.M., 2001, Vibration analysis of cross-ply laminated composite cylindrical shells using the wave propagation approach, *Applied Acoustics* **62**: 1221-1228.
- [32] Khalili S.M.R., Davar A., Malekzadeh Fard K., 2012, Free vibration analysis of homogeneous isotropic circular cylindrical shells based on a new three-dimensional refined higher-order theory, *International Journal of Mechanical Sciences* **56**: 1-25.
- [33] Shakeri M., Yas M.H., Ghasemi G.M., 2005, Optimal stacking sequence of laminated cylindrical shells using genetic algorithm, *Mechanics of Advanced Materials and Structures* **12**: 305-312.